

STRESS ANALYSIS OF MECHANICALLY FASTENED JOINTS AND STRESS INTENSITY FACTOR SOLUTIONS FOR COUNTERSUNK HOLES UNDER GENERAL LOADING

J.J.M. de Rijck^{*}, S.A. Fawaz⁺

The neutral line model is a simple analytical tool to calculate stresses in a lap-splice or butt joint. The method is verified by comparing analytical and experimental results. The model is based on advanced beam theory to calculate the displacements and accounts for the eccentricities inherent to a multi-layer joint. Adding the load transfer in this investigation provides a more physical realistic model. A mixture of monolithic and laminated joints were tested which provided a sound basis for stress comparison. Knowing the stresses at the most critical fastener row enables the analysis to do a more accurate fatigue crack growth prediction. For this prediction, stress intensity factors for countersunk holes need to be produced. In this investigation existing solutions are used to compare the method setup. A convergence study was performed and the new K solutions were compared to solutions in the literature.

INTRODUCTION

The neutral line model accounts for the eccentricities inherent in a multi-layer joint and uses advanced beam theory to derive the analytical solution for the in-plane and out-of-plane displacements that in turn can easily be converted to normal stress due to tension and bending in all structural elements in lap-splice or butt joints. The existing method was verified by using two lap-splice and two butt joints with properties similar to real aircraft joints, including the influence of longitudinal stiffeners. This validation proved that for a first approximation, the stresses close to the most critical fastener row could be accurately predicted. However, the existing model used an indirect method (fastener rotation) to include some fastener influence, and did not include a direct method to include the fastener load transfer. This new improved neutral line model includes a method based on the strain distribution, as a function of the applied load, in the overlap region of the joints and

^{*} Delft University of Technology, Aerospace Engineering, Structures and Materials Laboratory, 2629 HS, Delft, The Netherlands

⁺ United States Air Force Academy, Department of Engineering Mechanics, 2354 Fairchild Drive, Suite 6L-155, USAF Academy, CO 80840

fastener flexibility to calculate the stresses in the structural elements between the fasteners. This allows for a more accurate stress calculation at the most critical fasteners.

Included in this analysis are two materials, basic monolithic aluminum 2024-T3 and the Fiber Metal Laminate Glare. The latter is of special interest with respect to the application of Glare in the Airbus A380. Since Glare is a laminated material, it is of importance to know the stress distribution through the thickness, especially at the location of the fasteners. The material properties are different for each layer and therefore a stepped stress distribution through the thickness exists inside the material, this requires a somewhat different approach to calculating the variables inherent to joints such as joint eccentricity and rivet flexibility. Strain gage data at several locations in the overlap region was collected for the entire load range.

NEUTRAL LINE MODEL

The ‘classical’ neutral line model [1] is one-dimensional in such a way that the displacement of the neutral axis determines the behavior of the joint as a structural element. In this investigation the option of adding load transfer to the neutral line model was investigated. Load transfer in both adhesively bonded lap-splice and butt joints is straightforward since the load transfer is continuous in the overlap region and not discrete as in mechanically fastened joints. Three approaches are available to implement the ‘load transfer’ into the neutral line model; specifically, rivet rotation by Schijve [1], adjusting flexural rigidity by Müller [2] and adding an internal moment due to the eccentric load path in a mechanically fastened joint. The latter was investigated in this effort. Rivet rotation is not directly determined by the load transfer, the rivet rotation can account for added flexibility in a joint. For more information on the physical bases for rivet rotation, see [1] & [6]. The method proposed by Müller [2] is not chosen either since that method is based on changing the actual flexural rigidity to a virtual flexural rigidity. This method is adequate for joints made of monolithic materials, but does not allow for correct calculation of the neutral line displacements for fiber metal laminates because both the elastic modulus and moment of inertia are changed and thus not representative of the actual structure.

In this investigation, a neutral line model for Glare lap-splice and butt joints is developed. The derivation is straightforward but care must be taken in calculating the correct moments of inertia and stresses using the calculated displacements from the neutral line model.

The ‘classical’ neutral line model will be introduced by means of a lap-splice joint shown in Figure 1. The stresses in the area of interest are then easily obtained as shown below, starting with static equilibrium of the specimen. Point A can be found at the clamped left-side of the specimen:

⊥

□

$$\sum M_{Point A} = 0$$

$$M_a - M_b - Pa - D_b l_{tot} = 0 \quad (1)$$

Equilibrium for each separate “beam” part can be written as follows for the classical neutral line model, see figure 2:

$$(M_x)_i = M_a + Pw_i - D_a \left(\sum_1^i L_{i-1} + x_i \right) = (EI)_i \left(\frac{d^2 w}{dx_2} \right)_i \quad (2)$$

Introducing the internal moment to the neutral line model is based on the assumption that in a three-fastener row lap-splice joint as shown in figure 3, the load is not equally divided over all three-fastener rows. Since the strain distribution in the overlap region is not known and difficult to model as easily as the neutral line model, it is assumed that the line of action of the resulting force P coincides with the neutral axis throughout the lap-splice joint. When the load arrives at the first fastener row, part of the force is directed to the other sheet. Only in a perfect symmetrical 2 fastener row lap-splice joint will the load in both sheets be equal, in all other cases the loads in the sheets will be different. The sheets between the fasteners are assumed to act as one ‘beam’. To keep things simple and easy to implement in the neutral line model, an internal moment is required to account for the differences in load.

Rewriting Eqn. 2 to include the internal moment, according to figure 3:

$$(M_x)_i = M_a - M_i + Pw_i - D_a \left(\sum_1^i L_{i-1} + x_i \right) = (EI)_i \left(\frac{d^2 w}{dx_2} \right)_i \quad (3)$$

Or in a more useful form

$$\left(\frac{d^2 w}{dx^2} \right)_i - \alpha_i^2 w_i = \alpha_i^2 \left(\frac{M_a}{P} - \frac{M_i}{P} - \frac{D_a}{P} \left(\sum_1^i L_{i-1} + x_i \right) \right) \quad (4)$$

with
$$\alpha_i^2 = \frac{P}{(EI)_i}$$

and solving Eqn. 4 for the out of plane displacement, w_i ,

$$w_i = A_i \sinh(\alpha_i x_i) + B_i \cosh(\alpha_i x_i) + \left(\frac{D_a}{P} \left(\sum_1^i L_{i-1} + x_i \right) - \frac{M_a}{P} + \frac{M_i}{P} \right) \quad (5)$$

The boundary conditions in each part of the beam are

$$w_{j+1} = w_j + e_j \quad (6a)$$

⊥

□

$$\left(\frac{dw}{dx}\right)_{x_i=L_i} = \left(\frac{dw}{dx}\right)_{x_{i+1}=0} \quad (6b)$$

Part I

$$w_1 = A_1 \sinh(\alpha_1 x_1) + B_1 \cosh(\alpha_1 x_1) + \left(\frac{D_a}{P}(x_1) - \frac{M_a}{P}\right) \quad (7)$$

Substitution of the boundary conditions at $x_l = 0$, namely the displacement $w(x_l = 0)$ and the rotation $\left(\frac{dw}{dx}\right)_{x_l=0}$ are restricted due to the clamped edges of the lap-splice joint, in Eqn. (7) yields

$$B_1 = \frac{M_a}{P} \quad (8)$$

$$A_1 \alpha_1 = -\frac{D_a}{P} \quad (9)$$

Part II

$$w_2 = A_2 \sinh(\alpha_2 x_2) + B_2 \cosh(\alpha_2 x_2) + \left(\frac{D_a}{P}(L_1 + x_2) - \frac{M_a}{P} + \frac{M_2}{P}\right)$$

The displacement at the first fastener row for the 2nd beam is equal to the displacement of the 1st beam for $x_l = L_1$ plus the eccentricity jump. The eccentricity jump is the distance between the neutral axis of the 1st beam and the neutral axis of the 2nd beam. Using Eqn. (6a) & (6b):

$$w(x_2 = 0)_2 = w(x_1 = L_1) + e_1$$

$$B_2 = A_1 \sinh(\alpha_1 L_1) + B_1 \cosh(\alpha_1 L_1) - \frac{M_2}{P} + e_1 \quad (10)$$

$$\left(\frac{dw}{dx}\right)_{2,x_2=0} = \left(\frac{dw}{dx}\right)_{1,x_1=L_1}$$

$$A_2 \alpha_2 = A_1 \alpha_1 \cosh(\alpha_1 L_1) + B_1 \alpha_1 \sinh(\alpha_1 L_1) \quad (11)$$

Part III

$$w_3 = A_3 \sinh(\alpha_3 x_3) + B_3 \cosh(\alpha_3 x_3) + \left(\frac{D_a}{P}(L_1 + L_2 + x_3) - \frac{M_a}{P} + \frac{M_3}{P}\right)$$

From the 2nd to the 3th beam no eccentricity jump occurs ($e_2 = 0$), this since the moment of inertia of the 3th beam is equal to that of the 2nd beam. Should the

⊥

□

moment of inertia for both beams be different then the displacement at $x_3 = 0$ is equal to the displacement at $x_2 = L_2$ plus the eccentricity e_2 . Using Eqn. (6a) & (6b):

$$w(x_3 = 0)_3 = w(x_2 = L_2) + e_2$$

$$B_3 = A_2 \sinh(\alpha_2 L_2) + B_2 \cosh(\alpha_2 L_2) - \frac{M_3}{P} + \frac{M_2}{P} + e_2 \quad (12)$$

$$\left(\frac{dw}{dx} \right)_{3, x_3=0} = \left(\frac{dw}{dx} \right)_{2, x_2=L_2}$$

$$A_3 \alpha_3 = A_2 \alpha_2 \cosh(\alpha_2 L_2) + B_2 \alpha_2 \sinh(\alpha_2 L_2) \quad (13)$$

Part IV

$$w_4 = A_4 \sinh(\alpha_4 x_4) + B_4 \cosh(\alpha_4 x_4) + \left(\frac{D_a}{P} (L_1 + L_2 + L_4 + x_4) - \frac{M_a}{P} \right)$$

Using Eqn. (6a) & (6b)

$$w(x_4 = 0)_4 = w(x_3 = L_3) + e_3$$

$$B_4 = A_3 \sinh(\alpha_3 L_3) + B_3 \cosh(\alpha_3 L_3) + \frac{M_3}{P} + e_3 \quad (14)$$

$$\left(\frac{dw}{dx} \right)_{4, x_4=0} = \left(\frac{dw}{dx} \right)_{3, x_3=L_3}$$

$$A_4 \alpha_4 = A_3 \alpha_3 \cosh(\alpha_3 L_3) + B_3 \alpha_3 \sinh(\alpha_3 L_3) \quad (15)$$

Just as the edge at $x_1 = 0$ the edge of the specimen at $x_4 = L_4$ is clamped and thus restricted in movement. At $x_4 = L_4$ the displacement $w(x_4 = L_4) = a$ and the rotation $\left(\frac{dw}{dx} \right)_{x_4=L_4} = 0$. This results in the last two equations.

$$A_4 \sinh(\alpha_4 x_4) + B_4 \cosh(\alpha_4 x_4) + \left(\frac{D_a}{P} (L_1 + L_2 + L_4 + L_4) - \frac{M_a}{P} \right) = a \quad (16)$$

$$A_4 \alpha_4 \cosh(\alpha_4 L_4) + B_4 \alpha_4 \sinh(\alpha_4 L_4) + \frac{D_a}{P} = 0 \quad (17)$$

In the classic neutral line model, the internal moment is not considered ($M_i = 0$). M_i is the newly introduced internal moment dependent on the load transfer within the overlap region. Table 1 shows a summary of the system of 10 equations and 10 unknowns that need to be solved. After solving the set of equations, it is possible to calculate the stress at the desired location of the joint. In lap joints in transport

⊥

□

aircraft fuselage skins, the outer fastener row is critical; thus the stresses can be determined in the following manner.

$$M_{x=L_1} = M_a + Pw_{x=L_1} - D_a L_1 \quad (18)$$

With the bending moment known, it is possible to calculate the bending stress and the axial stress.

$$\sigma_b = \frac{M_{x=L_1}}{\frac{1}{6} W t_1^2} \quad (19)$$

$$\sigma_t = \frac{P}{W t_1} \quad (20)$$

With these stresses, the bending factor k can be calculated as:

$$k = \frac{\sigma_b}{\sigma_t} \quad (21)$$

To calculate the bending stress through the thickness, the following equation can be used:

$$\sigma_b(y) = \frac{M_{x=L_1} y}{I_{x=L_1}} \quad (22)$$

Using the calculated k (Eqn. (21)) for a certain joint geometry provides the stresses needed for the correct K -calculation. Figure (5) shows the relation between the applied stress and the bending ratio k on specimen 1. Assume that specimen 1 is subjected to cyclic fatigue where the applied stress is 100 MPa then the bending ratio $k = 1.66$, this means that the bending stress $\sigma_b = 166$ MPa at the most critical fastener row. These stresses are then used to calculate the stress intensity factor for a crack growing under this load condition. For accurate fatigue crack growth predictions, the pin-load and crack interaction are also important.

Internal Moment due To Load Transfer

Calculation of the internal moment for section 2 according to Figure 3: The total sum of the moment is taken about point “O”. The resulting force P on the right hand side of figure 3 does not contribute to the internal moment:

$$M_2 + P c_1 - (P - T_1) c_1 - T_1 (t_1 + c_4) = 0$$

$$M_2 = (t_1 + c_4 - c_1) T_1 \quad (23)$$

⊥

□

For internal moment in section $i = 3$:

$$\begin{aligned}
 -M_3 + (P - T_1 - T_2)c_1 + (T_1 + T_2)(t_1 + c_4) - P(t_1 + c_4) &= 0 \\
 M_3 &= (t_1 + c_4 - c_1)(P - T_1 - T_2)
 \end{aligned} \tag{24}$$

The unknown variables T_1 and T_2 can be calculated from the fastener flexibility as shown below.

Load Transfer and Fastener Flexibility

In order to find T_1 and T_2 , it is necessary to use an empirically derived fastener flexibility. In this derivation, the fastener flexibility by Swift [3] is used. Unfortunately, most of the empirical formulae in the open literature are for monolithic joints thus having the disadvantage that all sheets must have equal moduli of elasticity.

$$f_i = \frac{1}{Ed_i} \left[c_1 + c_2 \left(\frac{d_i}{t_{i,1}} + \frac{d_i}{t_{i,2}} \right) \right] \tag{25}$$

Combining the fastener flexibility with fastener stress equilibrium method mentioned in [4], results in the load transfer ratio γ_i

$$T_i = \gamma_i P \tag{26}$$

STRESS INTENSITY FACTOR SOLUTIONS FOR HOLES SUBJECTED TO COMBINED LOADING

Stress intensity factors are obtained using the *h-version* finite element method in conjunction with the 3-dimensional virtual crack closure technique to extract the K 's [5]. A detailed description is given in [6] on how the most optimized mesh generation procedure was developed. The first step in the ongoing investigation was to make sure we are able to produce accurate K factors for countersunk holes. The difference with [6] is that the latest convergence study is done using 20 noded solid elements. Increasing the degrees of freedom and introducing more integration points along an element edge.

Normalization of the calculated K 's is done using the following equations:

$$\beta = \frac{K}{S \sqrt{\frac{\pi a}{Q}}} \tag{27}$$

With Q known, K can be normalized:

⊥

□

$$\begin{aligned}
 Q &= 1 + 1.464 \cdot \left(\frac{a}{c}\right)^{1.65} \quad \text{for } \frac{a}{c} \leq 1.0 \\
 Q &= 1 + 1.464 \cdot \left(\frac{c}{a}\right)^{1.65} \quad \text{for } \frac{a}{c} > 1.0
 \end{aligned}
 \tag{28}$$

Knowing the exact stress state at the most critical fastener location allows for a detailed fatigue investigation using the calculated stresses from the neutral line model. Development of the stress intensity factor solutions will be discussed in this section.

Crack Growth

For an accurate fatigue crack growth prediction, exact stress intensity factors are essential. Currently, a large array of stress intensity factors for cracked countersunk holes subjected to tension, bending and bearing are being calculated. The crack shapes of interest are $0.100 < a/c < 10.0$, $0.05 < b/t < 0.50$, $0.10 < r/t < 4.00$; where a is the crack depth, c is the crack length, b depth of straight shank portion of countersunk hole, t sheet thickness, and r hole radius.

The next step is to build a complete database of stress intensity factors. A detailed description of how this is done can be found in [6]. At the moment a validation process is underway to determine the accuracy of the method and obtained solutions.

EXPERIMENTS

A mix of lap-splice and butt joints, nine specimens in all, representative of a large aircraft fuselage have been tested to obtain the load vs. strain data. Of these nine specimens, four were made of monolithic aluminum 2024-T3 and five were made from different Glare grades. See table 2 for the complete test matrix. In this paper the focus will be on three of the nine specimens, namely specimen 1, 3 and 5. Presenting more data would be repeating similar results as were obtained with specimen number 1, 3 and 5. All specimens were instrumented with KYOMA strain gages having a gage length of 2.0 mm, at locations similar to Figure 4.

For the discussion on the accuracy of the neutral line model, the focus will be on the strain gage data close to the most critical fastener row for each of the three specimens.

⊥

□

RESULTS

In order to compare stresses of the tested joints and the neutral line model, all the strains were converted to stress using one-dimensional Hooke's law. The stress at each measured location is the normal stress. This stress has to be decomposed into the tensile and the bending component with the following relation:

$$\begin{aligned}\sigma_t &= \frac{\sigma_i + \sigma_j}{2} \\ \sigma_b &= \frac{\sigma_i - \sigma_j}{2}\end{aligned}\tag{29}$$

The indices i, j are used to indicate the side of the sheet, since at most locations the strain gages are mounted back-to-back. Figures 6, 7 and 8 show the applied force vs. stress curves for specimens 1, 3 and 5.

Specimen 1

Figure 6 shows a comparison between the measured stresses and those calculated using the NLM. The influence of the load transfer can be better seen comparing the open symbols. The open symbols represent the linear tensile stresses and the non-linear bending stresses. The neutral line model calculated stresses compare within 10 % to the measured stresses. The tensile stresses differ 1%, the bending stresses for the 'classic' neutral line model not including the load transfer differ 13%. The improvement due to the load transfer is 5%, bringing the largest difference between the measurements and the predictions to 8% for the higher applied forces. For those higher forces, local deformations occur around the fastener holes.

Specimen 3

Figure 7 shows the applied force vs. stress for the butt joint. The same trend that could be seen for specimen 1 can be seen for specimen 3. The difference between the measured tensile stresses, the open squares, and the neutral line model prediction is 4% for the highest applied load. Again this indicates that the influence of plasticity around the fastener holes is significant [6]. For the bending stresses, the predictions for the 'classic' neutral line model differ 17%. The improvement obtained when the load transfer is included lowers the difference to 9%.

Specimen 5

Figure 8 shows the results for the Glare specimen. Here the difference between the measured tensile stresses and the calculated stresses is 2%. The calculated bending

stresses not including the load transfer differ 5%, including the load transfer, the difference between the measurements and the predictions is 1%.

Stress intensity factors

Figures 9-13 show the normalized K -solutions for 5 crack locations with $a/c = 0.50$, 0.75 and 1.00 , $b/t = 0.50$, 0.25 and 0.05 . The convergence study done to ensure numerical convergence of the FE solutions determines the minimum number of degrees of freedom. The difference between our results and those from [8] are based on the differences in the number of degrees of freedom. The smallest mesh used here contained 5 times the number of elements used in [8]; the largest mesh contained 50 times the number of elements. Both used 20 noded solid elements. The converged solutions can be found in figure 9-13.

CONCLUSION

A new derivation of the neutral line model to include load transfer through rivets was presented. At worst, the new model was within 10% of the measured stresses. For some configurations, the new model was within 0.2%. A possible improvement can be obtained when combining the fastener rotation to catch some effect of the plasticity effects around the fastener holes. This could explain the difference in accuracy between the monolithic aluminum joint and the glare joint.

The finite element models used provide the required accuracy needed for accurate K -solutions. Calculations are underway to fully populate the K solution database for all technically relevant a/c , r/t and b/t values .

ACKNOWLEDGEMENT

This work was funded by the Department of Defense (DoD) High Performance Computing Modernization Program (HPCMP) initiative through the Department of Defense's High Performance Computing Modernization Office (HPCMO) for the Computational Technology Area (CTA): Computational Structural Mechanics at the Engineering Research and Development Center (ERDC).

LIST OF SYMBOLS

a	=	Crack length/depth
a	=	misalignment of joint
c	=	Crack length
d	=	Diameter fastener

⊥

□

e_i	=	eccentricity jump for the i^{th} beam part
D_a	=	Reaction Force due to clamping
E_i	=	Modulus of Elasticity for the i^{th} beam part
f_i	=	Fastener flexibility
I_i	=	Moment of Inertia for the i^{th} beam part
P	=	Remote applied axial load
K	=	Mode I Stress Intensity Factor
L_i	=	Length of i^{th} part of the beam
L_{tot}	=	Total length of the joint
M_a	=	Moment due to clamping
M_i	=	Internal Moment due to load transfer
T_i	=	Fraction of load
t_i	=	Thickness of i^{th} beam part
W	=	Width of Specimen
β	=	Normalized K
σ	=	Remote applied stress
σ_b	=	Bending stress

REFERENCE LIST

- (1) Schijve, J., *Some Elementary Calculations on Secondary Bending in Simple Lap Joints*, NLR TR 72036, National Aerospace Laboratory, Amsterdam, NL, 1972
- (2) Müller, R. P. G., *An Experimental and Analytical Investigation on the Fatigue Behaviour of Fuselage Riveted Lap Joints, The Significance of the Rivet Squeeze Force, and a Comparison of 2024-T3 and Glare 3*. Dis. Delft University of Technology, 1995
- (3) Swift, T., *ASTM STP 486*, 1971, pp. 164-214
- (4) Homan, J.J., *Fatigue Damage Tolerance Methods for Joints in Fibre Metal Laminates*, Report B2-02-17, Delft university of Technology, Delft, to be published

⊥

□

- (5) Fawaz, S.A., *Fatigue Crack Growth in Riveted Joints*, Dis. Delft University of Technology, Delft University Press, 1997
- (6) Rijck, J.J.M. de, Fawaz, S.A., *Stress Intensity Factor Solutions for Countersunk Holes Subjected to Tension, Bending and Pin Loading*, 6th Joint DoD/FAA/NASA Conference on Aging Aircraft, 2002
- (7) Rijck, J.J.M. de, *Crack Interaction of Oblique Part-elliptical Through Cracks*, MS. Thesis, Aerospace Engineering, Structures & Materials Laboratory, August 1998
- (8) Newman, J.C. jr., Raju, I.S., *Stress-Intensity Factor Equations for Cracks in Three-Dimensional Finite Bodies Subjected to Tension and Bending Loads*, Computational Methods in the Mechanics of Fracture, Elsevier Science Publishers B.V., 1986

⊥

□

TABLE 1 Summary of Equations for Neutral Line Model with fixed clamping and misalignment.

Equation (8)	$B_1 = \frac{M_a}{P}$
Equation (9)	$A_1\alpha_1 = -\frac{D_a}{P}$
Equation (10)	$B_2 = A_1 \sinh(\alpha_1 L_1) + B_1 \cosh(\alpha_1 L_1) - \frac{M_2}{P} + e_1$
Equation (11)	$A_2\alpha_2 = A_1\alpha_1 \cosh(\alpha_1 L_1) + B_1\alpha_1 \sinh(\alpha_1 L_1)$
Equation (12)	$B_3 = A_2 \sinh(\alpha_2 L_2) + B_2 \cosh(\alpha_2 L_2) - \frac{M_3}{P} + \frac{M_2}{P} + e_2$
Equation (13)	$A_3\alpha_3 = A_2\alpha_2 \cosh(\alpha_2 L_2) + B_2\alpha_2 \sinh(\alpha_2 L_2)$
Equation (14)	$B_4 = A_3 \sinh(\alpha_3 L_3) + B_3 \cosh(\alpha_3 L_3) + \frac{M_3}{P} + e_3$
Equation (15)	$A_4\alpha_4 = A_3\alpha_3 \cosh(\alpha_3 L_3) + B_3\alpha_3 \sinh(\alpha_3 L_3)$
Equation (16)	$A_4 \sinh(\alpha_4 x_4) + B_4 \cosh(\alpha_4 x_4) + \left(\frac{D_a}{P} (L_{tot}) - \frac{M_a}{P} \right) = a$
Equation (17)	$A_4\alpha_4 \cosh(\alpha_4 L_4) + B_4\alpha_4 \sinh(\alpha_4 L_4) + \frac{D_a}{P} = 0$

⊥

□

TABLE 2 Overview of all specimens used to obtain load vs. strain data.

Specimen no.	type	face	Material	Thickness [mm]
1	Lap-splice Joint	sheet 1	Al 2024-T3	6.4
		sheet 2	Al 2024-T3	4.0
2	Lap-splice Joint	sheet 1	Al 2024-T3	2.5
		sheet 2	Al 2024-T3	2.0
3	Butt Joint	sheet 1, 2	Al 2024-T3	4.0
		butt strap	Al 2024-T3	4.0
4	Butt Joint	sheet 1, 2	Al 2024-T3	2.0
		butt strap	Al 2024-T3	2.0
5	Lap-splice Joint	sheet 1	Glare 3A-6/5-0.5	4.25
		sheet 2	Glare 4A-8/7-0.5	6.63
6	Butt Joint	sheet 1, 2	Glare 3A-6/5-0.5	4.25
		butt strap	Glare 2B-6/5-0.5	4.25
7	Butt Joint	sheet 1, 2	Glare 3A-8/7-0.3	4.15
		butt strap	Glare 2B-8/7-0.5	4.15
8	Butt Joint	sheet 1, 2	Glare 4A-5/4-0.5	4.0
		butt strap	Glare 2B-6/5-0.5	4.25
9	Butt Joint	sheet 1, 2	Glare 4B-5/4-0.5	4.0
		butt strap	Glare 2B-6/5-0.5	4.25

⊥

□

FIGURE 1 Nomenclature for neutral line model.

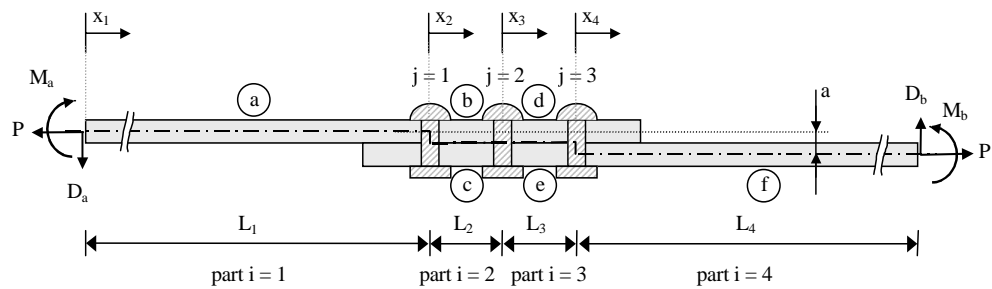
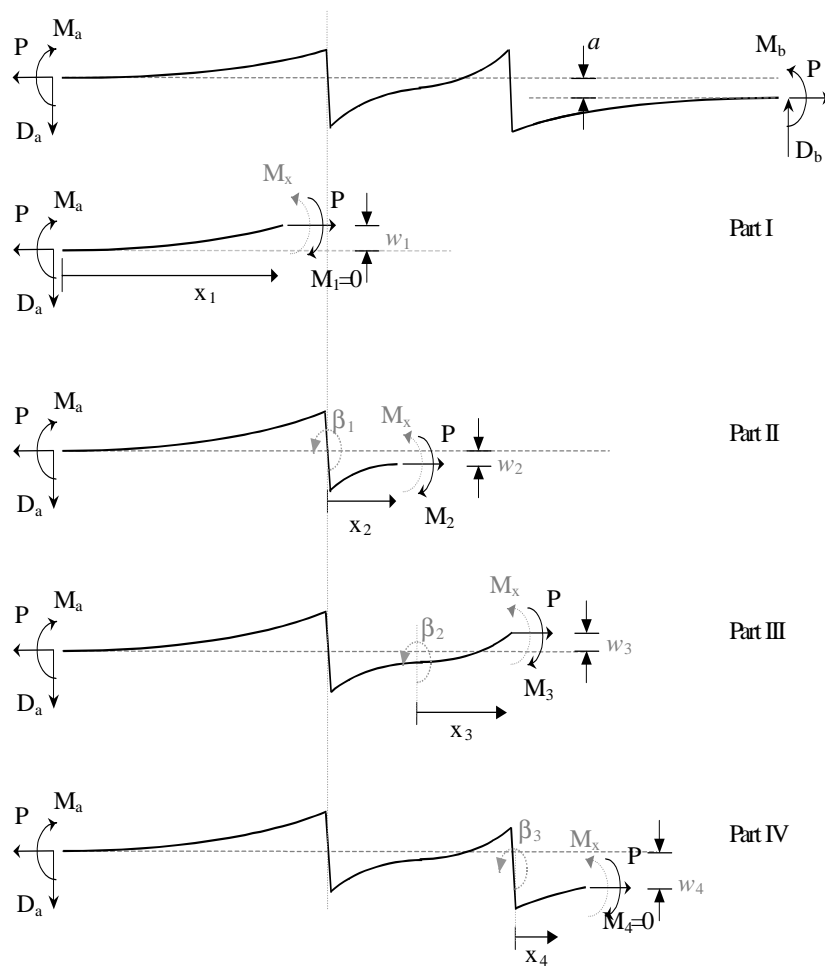


FIGURE 2 Deflection of neutral line for a three-rivet lap-splice joint.



⊥

□

FIGURE 3 Taking the actual load transfer into account requires an extra moment. Only the outer fasteners are shown, T_2 is thus the load transferred from sheet t_1 to sheet t_4 in the second fastener

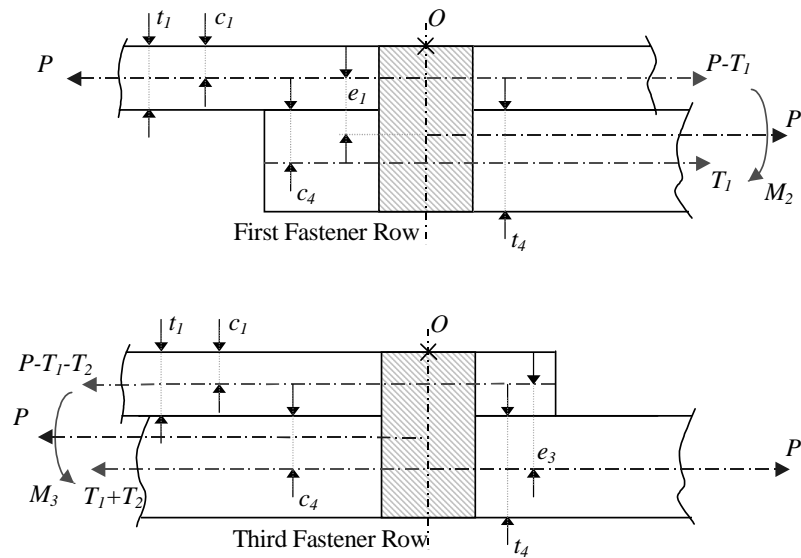
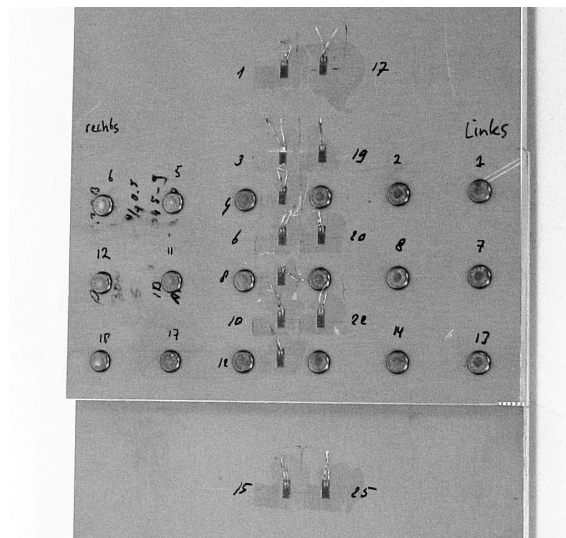


FIGURE 4 Location of instrumented strain gages



⊥

□

FIGURE 5 The Bending ratio (k) as a function of the applied stress on specimen 1

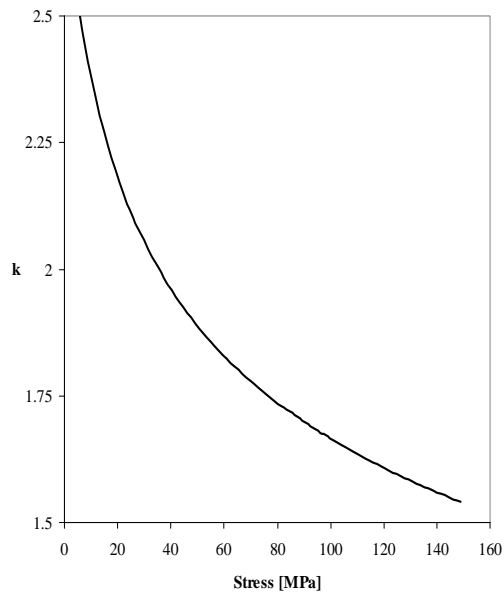
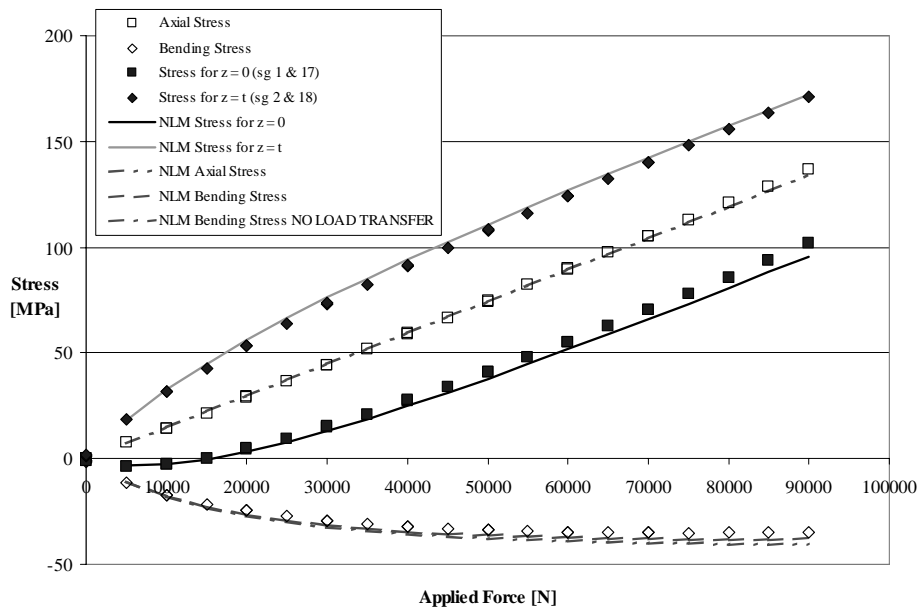


FIGURE 6 Specimen 1 lap-splice joint load vs. stress



⊥

□

FIGURE 7 Specimen 3 butt joint load vs. stress

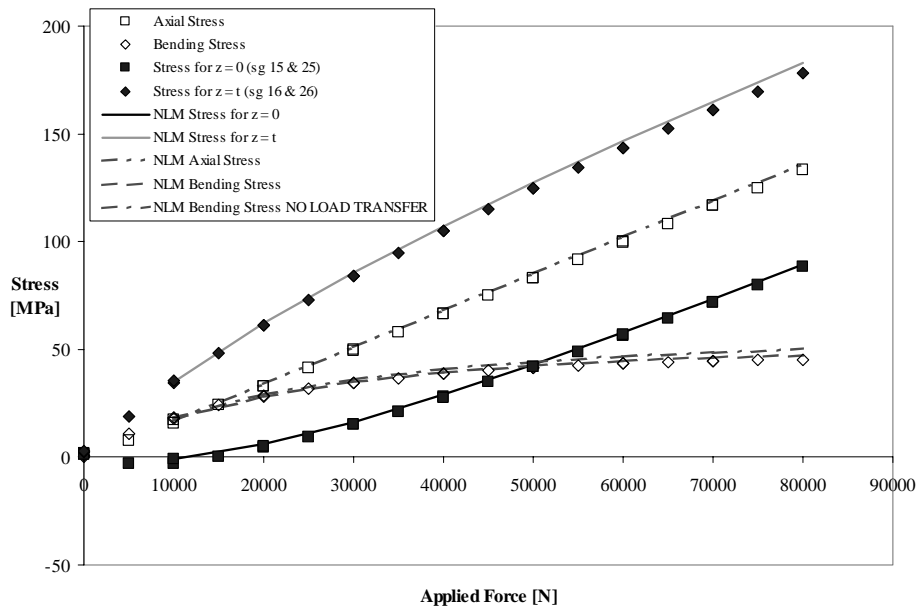
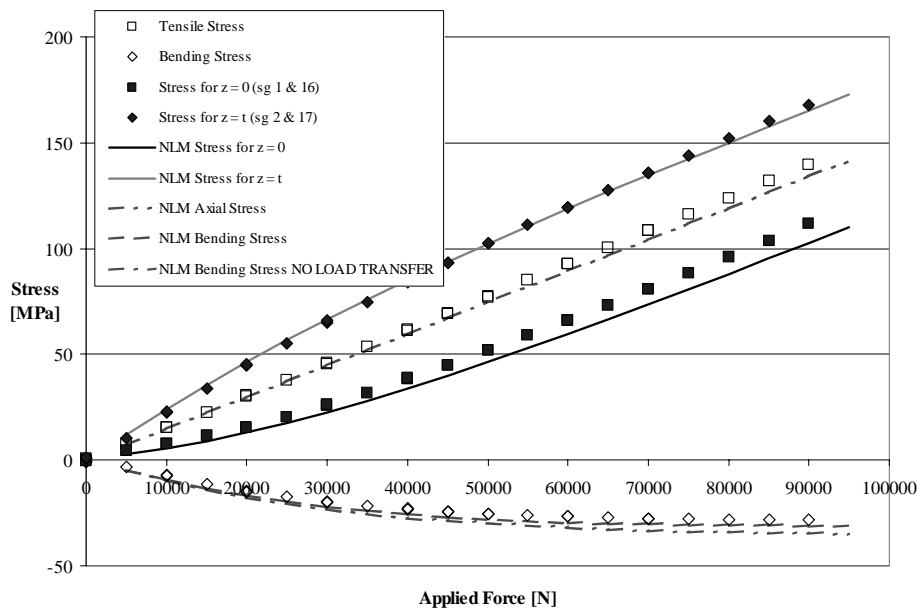


FIGURE 8 Specimen 5 lap-splice joint load vs. stress



⊥

□

FIGURE 9 Normalized K 's for crack location 1 under tension, $b/t = 0.50$

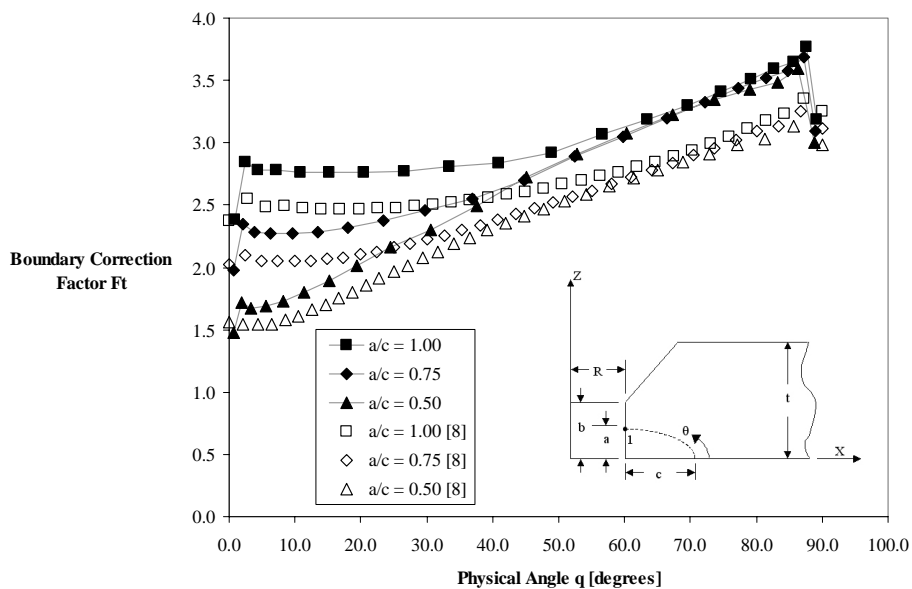
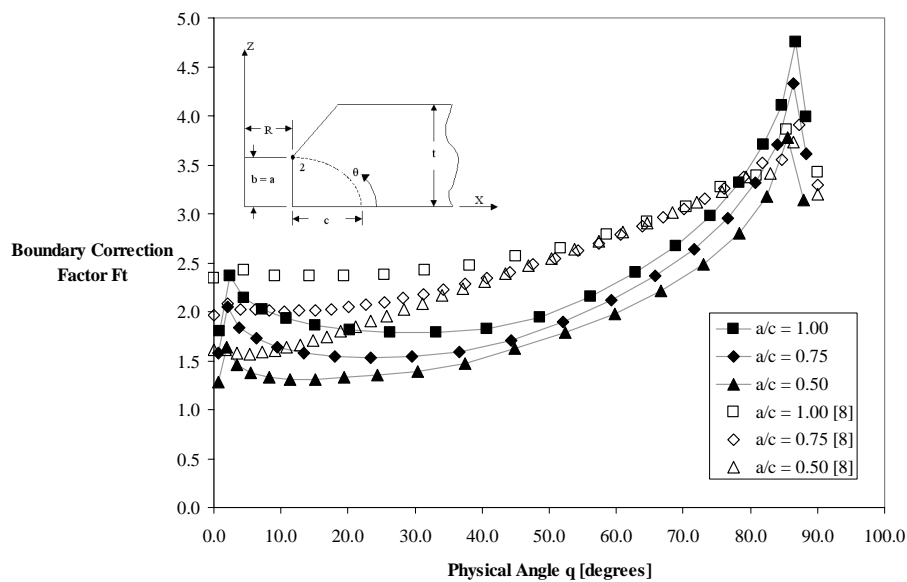


FIGURE 10 Normalized K 's for crack location 2 under tension, $b/t = 0.50$



⊥

□

FIGURE 11 Normalized K 's for crack location 3 under tension, $b/t = 0.50$

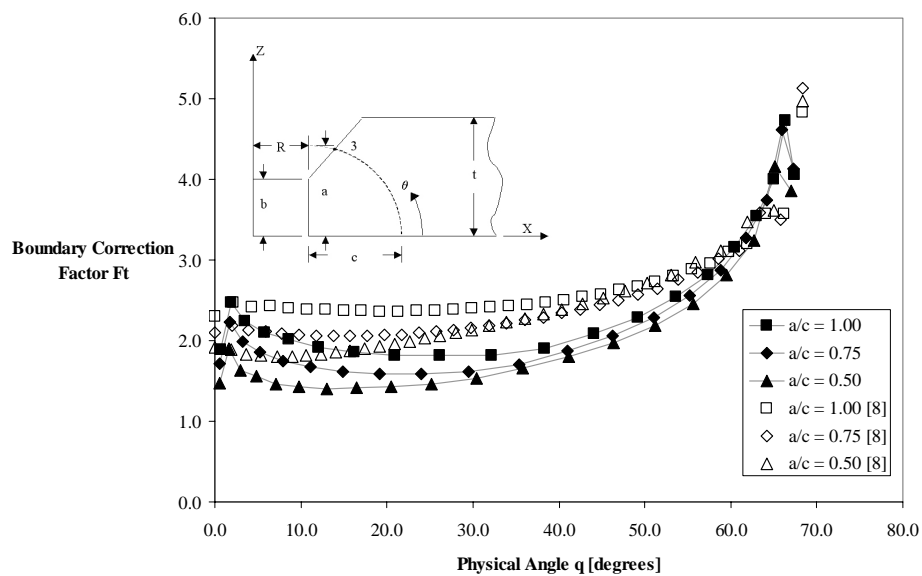
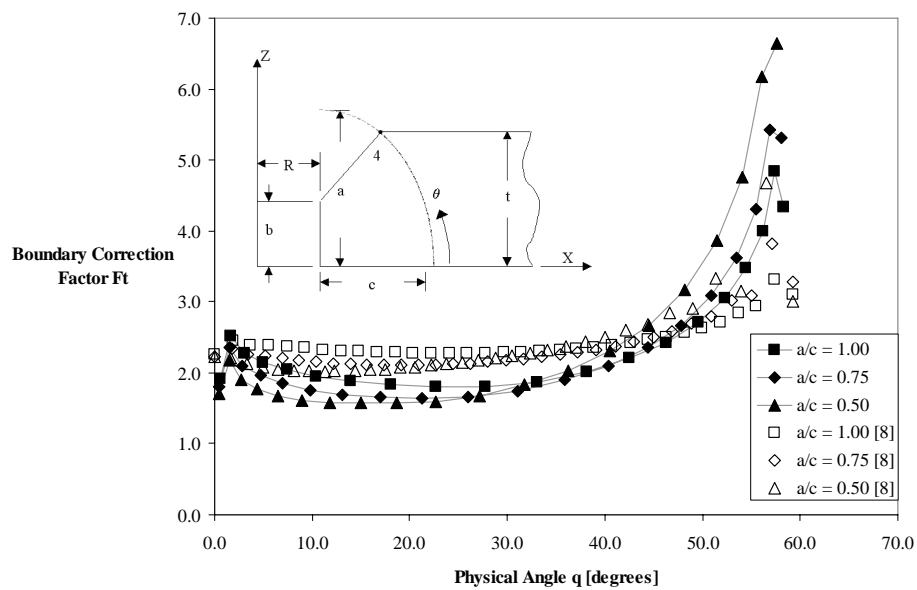


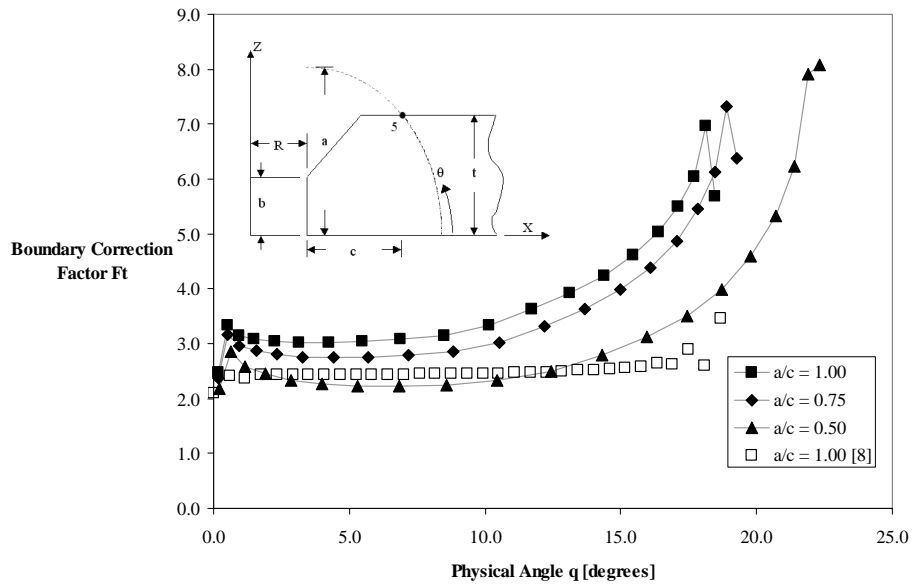
FIGURE 12 Normalized K 's for crack location 4 under tension, $b/t = 0.50$



⊥

□

FIGURE 13 Normalized K 's for crack location 5 under tension, $b/t = 0.50$



⊥

□